6

Power Drawn by Impellers in Multiple Impeller Systems

In designing a multiple impeller agitated gas-liquid contactor, power drawn by each impeller becomes the most important parameter, because the data of power drawn by each impeller is directly related to the flow patterns, circulation of liquid, turbulence, mass transfer and the status of gas dispersion in the system.

6.1 Power Drawn by Impellers in Ungassed Agitated Systems

6.1.1 Single impeller system

For a single impeller vessel, the classical approach of Rushton et al. resulted in the well-known Rushton chart of power number, N_P , vs. Re as shown in Fig. 6.1-1. Where N_P is defined as the power number, $N_P=P_g/(\rho N^3D^5)$. The plot can be expressed as

$$N_P = \frac{A}{Re} + B + \frac{C}{Fr} \tag{6.1-1}$$

Here A, B, and C are constants.

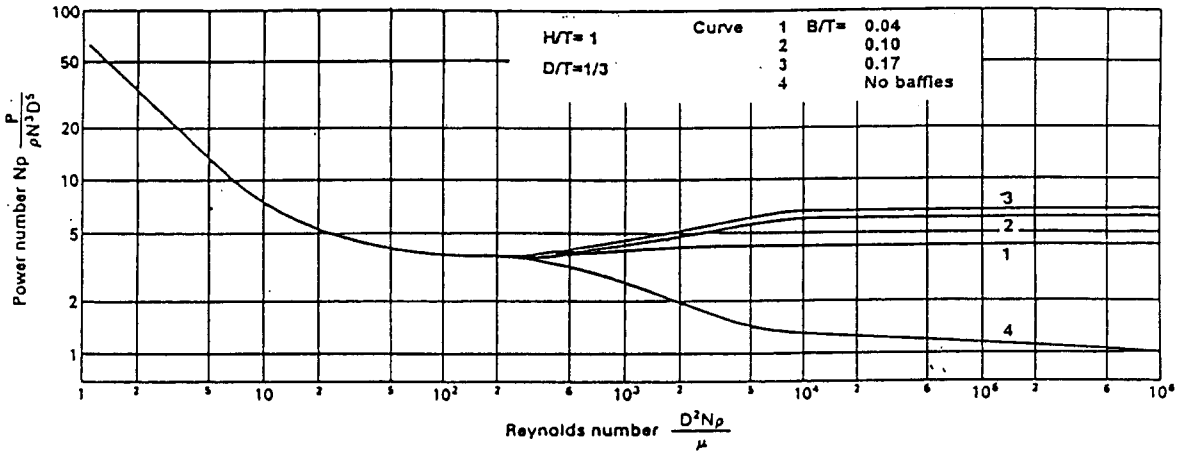

Fig. 6.1-1 Power number as a function of Reynolds number for a Rushton turbine impeller system with various baffle structures.

If the viscous effect is dominant, the inertia and gravity forces can be neglected and Eq. (6.1-1) becomes

$$N_P = A(Re)^{-1} \tag{6.1-2}$$

In the turbulent region or Re is larger than 10^4, the effect of the inertia force is dominant and the expression is reduced to:

$$N_P=B \qquad (6.1\text{-}3)$$

Therefore, in turbulent flow regime, the power is proportional to density of fluids and the third power of the rotational speed of impeller and fifth power of impeller diameter D.

For the system equipped with an axial flow impeller of the same diameter, the power drawn is always less than that those drawn by the radial flow impeller. The impeller without disc plate eliminates the interference to the liquid flow around the impeller, hence reduces the power consumption. In addition, the hydrofoil shape of the blade such as A310 or A315, which lessens the shear force of the impeller acting on the liquid can reduce the power demand further. Under ungassed conditions, the power drawn by the impeller increases with the magnification of the impeller size.

6.1.2 Multiple impeller system

In a multiple impeller system, the power drawn by each impeller will vary with the variation of the distance between impellers. It is well recognized that under an ungassed condition, the power drawn by each impeller can be seen similar to that drawn by an independent impeller if the distance between two neighboring impellers is larger than 1.5 times of impeller diameter. Fig.6.1-2 shows the total power drawn by the impellers in a dual Rushton turbine impeller system, which verifies the above statement.

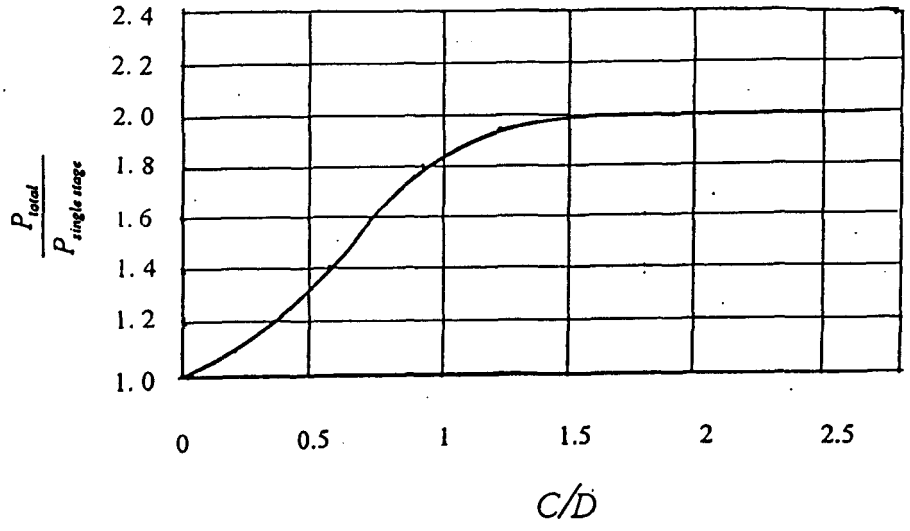

Fig. 6.1-2 $P_{total}/P_{single\ stage}$ vs. impeller distance in a dual impeller system.

For a triple impeller system equipped with the same impellers, the total power drawn by the system can be approximated as the sum of the power drawn by individual impeller if the impeller spacing is larger than 1.5D, while, in the system equipped with hybrid impellers, especially for the combination of radial and axial flow impellers, the total power drawn will

be reduced more or lesss even the impeller clearance is larger than 1.5D since the flow of axial impeller reduces the resistance of the upper incoming liquid.

6.2 Effect of Gassing on the Power Drawn by Impellers

6.2.1 Gassed power drawn by different impellers in single impeller system

Rushton turbine impeller

Since Rushton (1946) proposed the specific design of 6-straight-blade disk turbine impeller (as shown in Fig. 2.2-1(a)), it has been adopted extensively. Many researches (Rennie & Valentin, 1968; Van't Riet & Smith, 1973 and Nienow & Wisdom, 1974) had indicated that due to the distinctive structure of the Rushton turbine impeller, it is appropriate to be used in a gas-liquid mechanical agitated vessel. First, the appropriate blade pitch makes the Rushton turbine impeller to develop the strong trailing vortex, which can disperse gas effectively. Secondly, the disc structure of the Rushton turbine impeller precludes the sparged gas from rising along the shaft to the liquid surface directly, which is sucked into the trailing vortex to be dispersed. Finally, the strong recirculation flow caused by the Rushton turbine impeller conveys the dispersed bubbles back into the impeller region, which not only increases the efficiency of gas utilization, but also results in a better gas dispersion.

Early studies for gassed power consumption for mechanically agitated vessels were mostly reported in the form of P_g/P_o against the aeration(gassing) number Q_S/ND^3. Oyama and Endo (1955) reported that the ratio of gassed power draw to ungassed power draw for a single impeller drops drastically from 1.0 to 0.4 as gas flow number varies from 0.035 to 0.05. Calderbank(1958) postulated that the plot can be divided into two different straight line as

$$\frac{P_g}{P_o} = 1.0 - 12.6N_A \qquad \text{for} \qquad N_A<0.035 \tag{6.2-1}$$

and

$$\frac{P_g}{P_o} = 0.26 - 1.85N_A \qquad \text{for} \qquad N_A>0.035 \tag{6.2-2}$$

Since then, numerous modifications were presented by different authors, the most popular correlation adopted for estimating gassed power for a single impeller system is Michel and Miller's(1962) correlation as shown in Fig. 6-2-1 and can be written as:

$$P_g = C\left(\frac{P_o^2 ND^3}{Q_S^{0.56}}\right) \tag{6.2-3}$$

where C is a constant and it is dependent of impeller type. C=0.08 for a six-blade standard disk turbine if P_o and P_g are expressed in HP, N in rpm, D in ft and Q_S in ft^3/min. In SI units,

Mochizuki recommended the correlation given by Fukuda et al.(1968) is better for practical purpose, i.e.

$$P_g = 6.35\left(\frac{P_o^2 N D^3}{Q_S^{0.08}}\right)^{0.39} \qquad (6.2\text{-}4)$$

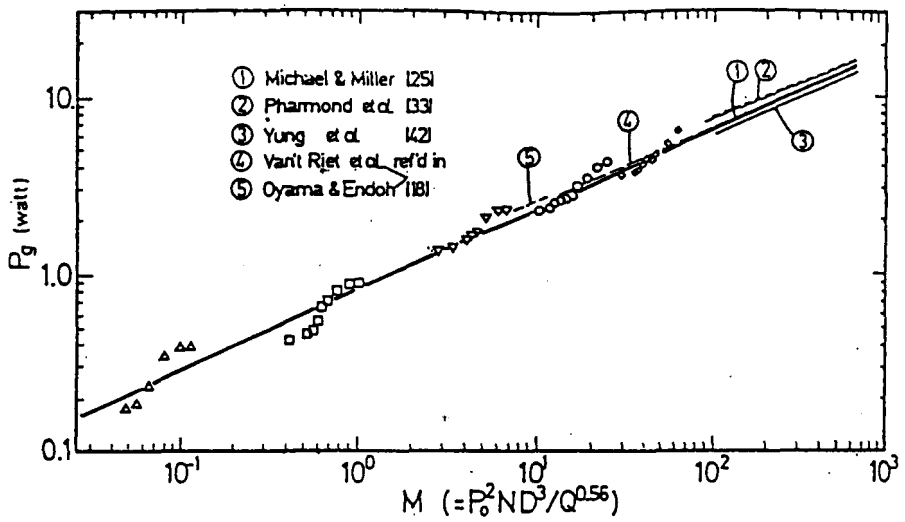

Fig. 6.2-1 Michel and Miller's correlation with Lu's experimental data

Since the gassed power drawn by the Rushton turbine impeller always decreases seriously with the increase in gassing rate, it is difficult to avoid the unstable power loading to the electrical motor during operation. When the gassing rate changes, the power dawn by the Rushton turbine impeller varies, which may exerts some damage on these mechanical equipment, such as sealings and gear box, etc..

Smith turbine impeller

Even though there are many advantages coming with the Rushton turbine impeller, the serious reduction in power drawn with an increase in aeration rate induces troubles in design and operation of the gas-liquid contactor, which makes the mechanical design of the system complex and expensive. Recently, many researchers (Nienow, 1990; Baker et al., 1994; Nienow, 1996; Vlaev and Martinov, 1999) postulated that the power drawn by the concave-blade disk turbine impeller (also known as the Smith turbine impeller or Scuba impeller and as shown in Fig.2.2-1c) was little affected by the variation of the aeration rate, and can handle much higher gassing rates. They pointed out that the flooding condition still does not appear to the Smith turbine impeller even under a larger aeration rate, i.e. the flooding phenomenon for the Smith turbine impeller happens only at an extremely large gassing condition. This fact implies that the Smith turbine impeller may has a better gas handling capability than the other traditional impellers and can be applied to the situation with a higher aeration rate, which is

conducive to the mass transfer performance and product yield.

Figure 6.2-2 shows the variation in the measured gassed power ratio (P_g/P_o) against the aeration number (Q_S/ND^3) for the Smith turbine impeller and the Rushton turbine impeller. The power drawn data of the Smith turbine impeller obtained by several researchers (Bakker et al., 1994; Serafim & Martin, 1999) were also shown in this figure for comparison. From the plots shown in this figure, it can be found that the power drawn by the Smith turbine impeller only decreases slightly with the increase in the aeration rate, which is much different from what is seen for the Rushton turbine impeller. Based on this result, one may conclude that aeration only has a limited impact on the cavity type and size behind the leading blade of the Smith turbine impeller and the liquid pumping capacity of this impeller is not much affected by the gassing rate. Comparing to the Rushton turbine impeller, it is found that the power ratio of the Smith turbine impeller keeps almost unchanged for considerable gassing range, while the Rushton turbine impeller shows a sharp reduction in P_g/P_O even at lower gassing rates.

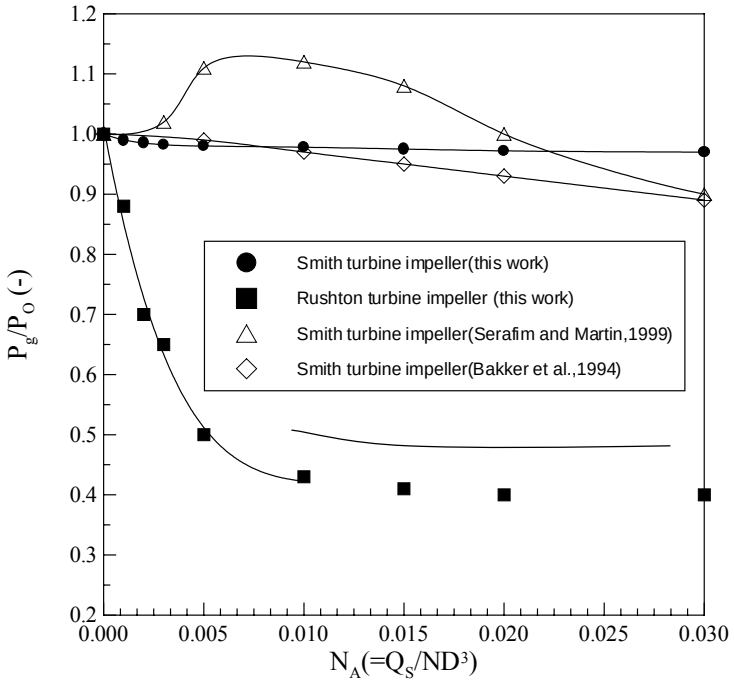

Fig. 6.2-2 The plots of P_g/P_o vs. aeration number N_A for the Rushton turbine impeller and the Smith turbine impeller.

In the above equations described here, P_g is always expressed as a function of the aeration number, which does not cover all the gas sucked in by the impeller, therefore it is not an appropriate variable used to correlate the gassed power. It is well understood that the gassed power is directly affected by the amount of gas involved at the vicinity of the impeller and the gas flow number consider only the sparging gas rate from beneath of the impeller. To

have the total amount of gas enter the vicinity of the impeller requires a quantitative analysis of gas recirculation and the nature of the cavity under the given operating conditions.

6.2.2 Gassed power drawn by impellers in multiple impeller systems

In contrast to a single impeller system, power drawn by each impeller in a multiple impeller system under a gassed condition has not been well discussed until recently (Nienow and Lilly, 1979; Kuboi and Nienow, 1982; Nishikawa et al., 1984; Machon et al. 1985; Roustan, 1985; Smith et al., 1987; Mochizuki et al., 1997; Lu and his coworkers, 1992, 1995, 1996). Since the non-uniform gas loading and gas recirculation rate, which are caused by the radial flow of the disk turbines, exist among each impeller in the multiple impeller system, this fact results in the gassed power drawn by each impeller in a multiple impeller system is quite different each other.

This argument is more applicable for the case of predicting the gassed power drawn by the upper impellers of a multiple impeller systems. It is well acknowledged that the gassed power drawn by the lowest impeller is very similar to that of a single impeller system; however, the gassed power drawn by the upper impellers are different depending on the how much gas is entrapped or recirculated into the impeller region. Figure 6.2-3 (Mochizuki, 1992) shows a plot of P_g/P_o vs. N_A, for the lower and the upper impeller in a dual turbine impeller system. The decrease in P_g/P_o, for the upper impeller is much slower than that of the lowest impeller, which nearly coincides with the trend seen for a single impeller system. This fact implies that the gas entrapped into the upper impeller region is much less than the amount of gas existing in the area surrounding the lower impeller. By measuring the gassed power for each impeller in dual and triple impeller systems, Lu and Yao(1992) pointed out that only 30~40% of the sparged gas enters the vicinity of the upper or middle impeller. This trend of the decrease in P_g/P_o vs. N_A tends to coincide with the path of the same plot of the single impeller system if the pumping capacity of the impeller increases, which accelerates the recirculation of gas bubbles.

To predict the gassed power drawn by the upper impeller in a dual impeller system, Nienow and Lilly (1979) proposed the equation as

$$(P_g)_{n=2} = P_o(1-\varepsilon_H) \tag{6.2-5}$$

where P_o is the ungassed power and ε_H is the gas hold-up of the system. Although several research efforts (Machon, 1985; Abrardi, 1988; Hudcova et al., 1989) confirmed the applicability of Eq. (6.2-5), practically it is impossible to know the value of ε_H before having a real stirred vessel.

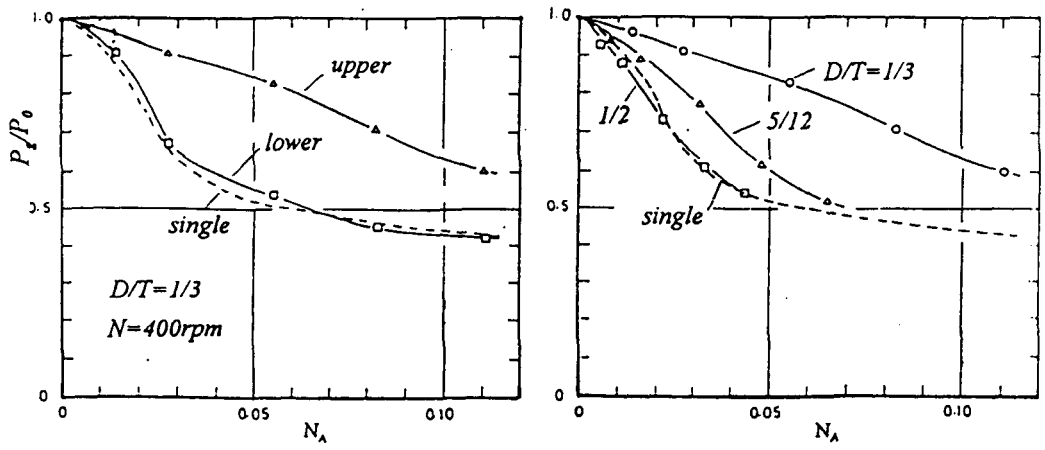

Fig. 6.2-3 P_g/P_o vs. N_A for a dual turbine impeller system (Mochizuki, 1992)

Without considering the non-uniform distribution of gas bubbles within a multiple impeller system, Nocentini(1988) concluded that the gassed power drawn by the upper impellers is the same and is corresponding to the power drawn in a single impeller provided gas is uniformly sparged over entire bottom surface of the tank. This conclusion may be true for a gas flow rate is large enough, and a pumping rate of the impeller strong enough, to uniformly distribute the bubbles to the entire vessel. A similar conclusion was also given by Linek et al.(1996) that the gassed power drawn by each impeller is the same and is a function of the superficial gas velocity. More quantitative studies are conducted in the laboratory at NTU to examine how the amount of recirculation of bubbles will affect the gassed power drawn by the upper impellers.

Recently, Cui et al.(1996) have correlated the data obtained by several researchers and presented two different equations, in which the transition occurs at P_g/P_o =0.5 for the top and middle impellers. They mentioned that the behavior of the top and middle impellers in a multiple impeller system are nearly identical. By adopting the CFD method to depict the path of the motion of bubbles, Lu and Chiu(1995) evaluated the fraction of the originally fed gas flowing through the upper impellers and found that the fraction of the fed air flowing through each impeller is quite different, which clearly indicates the non-uniform gas loading of the middle and upper impellers in the multiple impeller systems.

6.2.3 Recirculation of gas around impellers

Single impeller system

Figure 6.2-4 shows the calculated gas recirculation rates for a single Rushton impeller system of tank diameter T=0.141m under various rotational speeds and gassing rates (Lu and Wu, 2000). It is seen that no matter what the rotational speed is, the gas recirculation rate curves can be divided into three parts, i.e. low aeration rate ‘region A’, higher aeration rate

'region B' and flooding aeration rate 'region C'. In region A, the gas recirculation rate always increases sharply with the increase in gassing rate, under which the sparged gas is dispersed completely into small bubbles and most of bubbles are recirculated back into impeller region. However, once the gassing rate exceeds the peak values of these plots and entering region B, the gas recirculation rate decreases as the gassing rate increases. From the experimental observation, it is found that the status of gas dispersion has changed from complete gas circulation around the whole vessel to the gas circulation confined to the upper part of the system as described by Nienow et al. (1977). Calculating the value of gas flow number $N_A=Q_S/ND^3$ corresponding to the peak points of these curves, it is found that N_A at this point is always approximately equal to 0.03, which discriminates the appearance of the large cavity around the impeller as pointed out by Warmoeskerken and Smith (1988). Under such a condition, only a fraction of sparged gas is recirculated back into impeller region and the other sparged gas rises up to the free surface along the tank wall. This fraction of the recirculated gas decreases with the increase in sparged gas rate. With a further increase in gassing rate and entering region C, the gas recirculation rate will sharply decrease and approach zero due to the occurrence of the flooding phenomenon. Since the increase in the rotational speed of the impeller will increase the pumping capacity, it also increases the rate of gas recirculation, as a result, the span of the region A and B increases as shown in Fig 6.2-4.

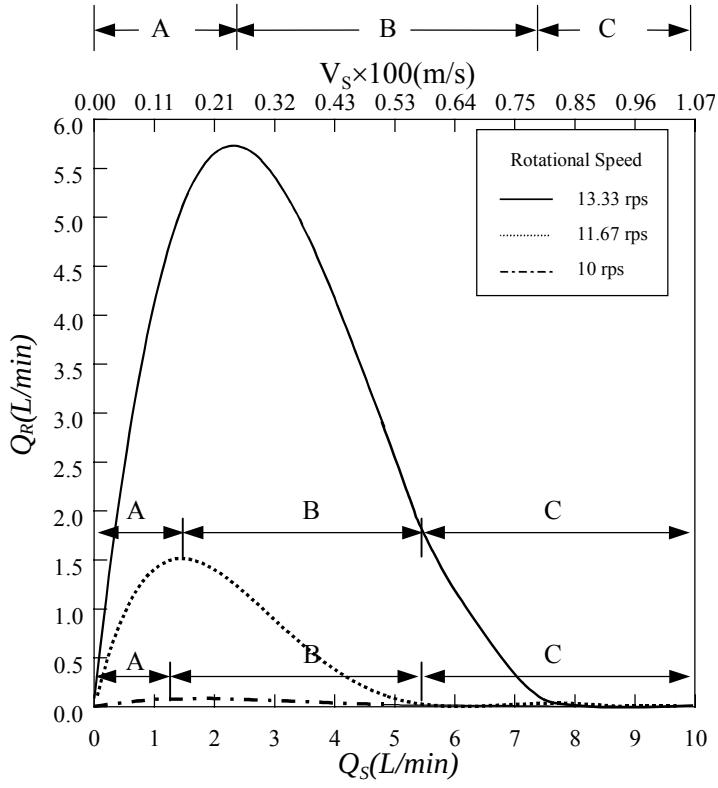

Fig. 6.2-4 Effect of the aeration rate on the gas recirculation rate in the single Rushton turbine impeller system.

Since the liquid pumping rate of impeller can be estimated by:

$$Q_L = \pi D \int_{-w/2}^{w/2} V_r dz \qquad (6.2\text{-}6)$$

where V_r is the radial velocity distribution along the vertical plane at the impeller blade tip. By plotting the liquid pumping rate Q_L at the peak points of each curve shown in Fig. 6.2-4 against the corresponding gas superficial velocity, it is found that all the points settle in a straight line as shown in Fig. 6.2-5, which maps the gas dispersion status within stirred tanks. In the region above this line, gas bubbles are well circulated in the whole vessel and no large cavity appears around the impeller, while in the region below this line, gas circulation appears only in the upper part of the stirred vessel and large cavity compasses the impeller blade.

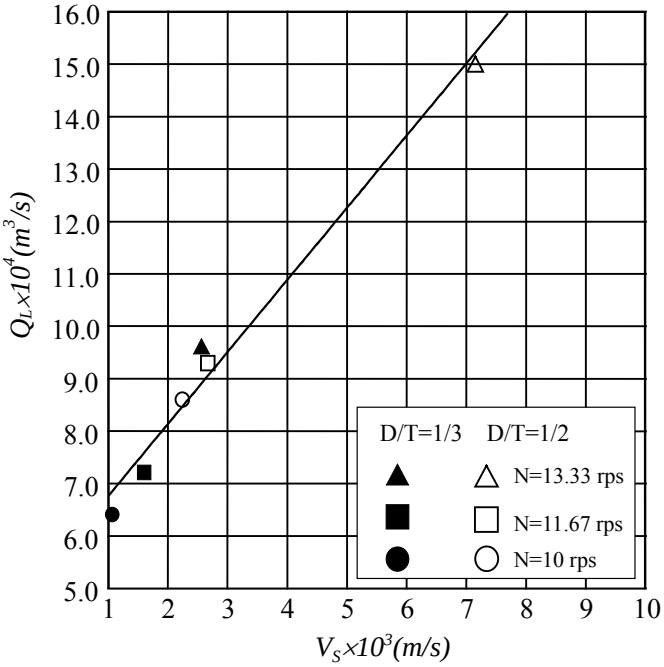

Fig.6.2-5 Plot of liquid pumping rate vs. V_S at the maximum gas recirculation rates.

To examine the effect of D/T ratio on the gas recirculation rate around impeller, the gas recirculation rates are evaluated for the systems equipped with a single Rushton turbine impeller having different diameters (i.e. D/T=1/3 and 1/2) and the results are plotted in Fig. 6.2-6. The plots in this figure point out that (1) gas recirculation rate increases sharply with sparged gas rate under a lower gassing rate and passes through a peak value at a certain gassing rate, and finally approaches zero when the impeller becomes flooded; (2) the impeller with a larger diameter recirculates more gas into impeller region under the same rotational speed, which is consistent with the results presented by Mochizuki (1992). The relationship between the liquid pumping rate of impeller with a larger diameter and the gas superficial velocity at the maximum gas recirculation rates obtained in Fig. 6.2-6 were also plotted in Fig.

6.2-5. It is found that all the data points settle on this single straight line, which demonstrates that the pumping capacity of impeller governs the gas recirculation phenomenon.

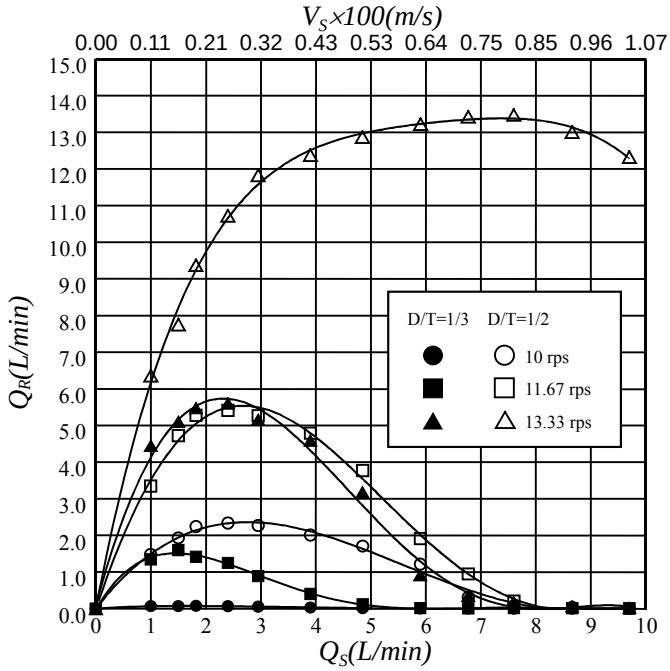

Fig. 6.2-6 Comparison of the gas recirculation rate for the impeller with different diameters in the single impeller system.

For the single Rushton turbine impeller system, the gas recirculation rate Q_R increases with the rotational speed N, the sparged gas rate Q_S and the D/T ratio under lower aeration conditions (i.e. N_A<0.03). In this situation, the gas recirculation rate Q_R can be related to N, Q_S and D/T as:

$$Q_R/Q_S=0.95\,N^{2.85}Q_S^{0.13}(D/T)^{4.01} \qquad N_A=Q_S/ND^3<0.03 \tag{6.2-7}$$

However, as the sparged gas rate becomes larger (i.e. N_A>0.03), Q_R still increases with N and D/T, while gas recirculation rate decreases quickly with the increase in the aeration rate Q_S and the correlation is shifted as:

$$Q_R/Q_S=0.043\,N^{1.05}Q_S^{-1.12}(D/T)^{9.15} \qquad N_A=Q_S/ND^3>0.03 \tag{6.2-8}$$

The deviation of the results estimated by Eqs. (6.2-7) and (6.2-8) are less than 12%.

For a pitched blade impeller, if sparged gas rate is too small to load the impeller (Q_S/ND^3<0.03), gas will enter the impeller region only through recirculation. In this situation, the impeller always can disperse gas effectively and the gas recirculation rate increases with the increase in sparged gas rate. However, once the sparged rate exceeds a certain value (Q_S/ND^3>0.03), the gas loads to the impeller directly. Under this condition, it is observed that gas can not be dispersed completely and the gas recirculation rate decreases with the increase in the sparged gas rate. Increasing the D/T ratio, the gas recirculation rate around the pitched

blade impeller always becomes larger regardless of gas loading regimes. Figure 6.2-7 shows the comparison of the calculated gas recirculation rates for the single Rushton turbine impeller system and the single pitched blade impeller systems with a N=13.3 rps and various sparged gas rates. It is found that the trend of the variation of Q_R for the pitched blade impeller is very similar to that for the Rushton turbine impeller. In other words, Q_R increases with the increase in Q_S and passes through a peak value and approaches zero once the impeller becomes flooded. When the impeller disperses gas effectively ($Q_S/ND^3<0.03$), the pitched blade impeller always gives a larger Q_R than the Rushton turbine impeller due to its strong circulation flow, while the Rushton turbine impeller provides a higher gas recirculation rate under a higher gassing condition owing to its better gas dispersion capability. Summarizing the calculated gas recirculation rates around the pitched blade impeller under various operating conditions, the following formulas are obtained to estimate Q_R around the pitched blade impeller for two different gas loading regimes as:

$$Q_R/Q_S=1.05N^{2.91}Q_S^{0.31}(D/T)^{5.01} \quad \text{for indirect gas loading i.e. } Q_S/ND^3<0.03 \quad (6.2\text{-}9)$$

$$Q_R/Q_S=0.051N^{0.95}Q_S^{-1.05}(D/T)^{9.52} \quad \text{for direct gas loading i.e. } Q_S/ND^3>0.03 \quad (6.2\text{-}10)$$

The deviations of the above two correlation equations are less than 15%

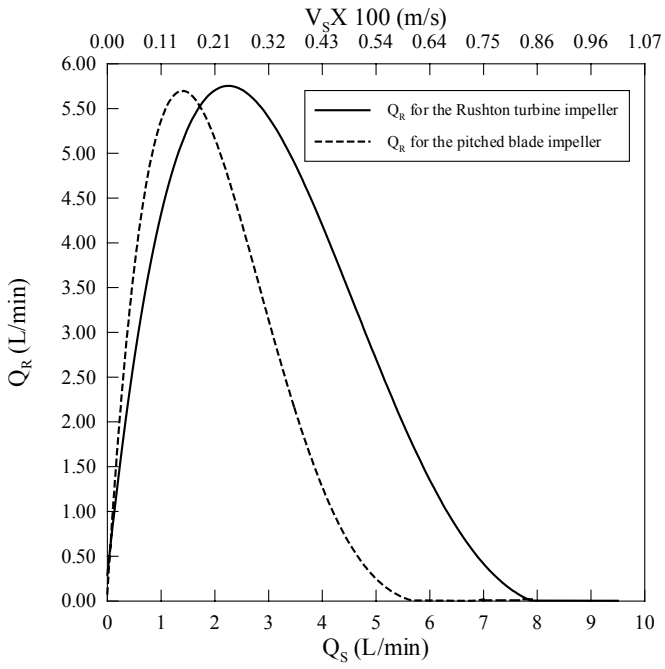

Fig. 6.2-7 Comparison of the gas recirculation rate for the Rushton turbine impeller and pitched blade impeller in the single impeller system with N=13.3 rps.

Multiple impeller system

Prior to estimate the gas recirculation rate for impeller at each stage, Q_{Rn} in a multiple impeller system, it is necessary to acquire the net sparged gas rate entering each impeller from

underneath directly, Q_{Sn}, which can be approximated numerically by combining the gas flow velocity and gas holdup as shown in Chap.4. Since only the up-flowing gas enters the impeller region from underneath, only the grid cells possess the upward axial velocity of gas flow are taken into account during estimating the net sparged gas rate for upper impellers. Simulating the gas-liquid flow fields of RRR, PRR, PPR and PPP impeller systems under various operating conditions, i.e. various rotational speed N, the original sparged gas rate Q_{S1} and the D/T ratio, the net sparged gassing rate around each impeller Q_{Sn} for each system can be calculated.

By correlating Q_{Sn}/Q_{S1} with N, Q_{S1}, the impeller stage n_s and the D/T ratio, four different formulas for predicting the net sparged gas rate for each upper impeller Q_{Sn} ($n_S \geq 2$) in the RRR, PRR, PPR and PPP impeller systems are be given as:

$$Q_{Sn}/Q_{S1}=105.1N^{-0.28}Q_{S1}^{0.25}n_s^{-0.474}(D/T)^{1.69} \quad \text{for RRR impeller system} \quad (6.2\text{-}11)$$

$$Q_{Sn}/Q_{S1}=35.3N^{-0.29}Q_{S1}^{0.22}n_s^{-0.512}(D/T)^{1.65} \quad \text{for PRR impeller system} \quad (6.2\text{-}12)$$

$$Q_{Sn}/Q_{S1}=31.2N^{-0.31}Q_{S1}^{0.21}n_s^{-0.721}(D/T)^{1.63} \quad \text{for PPR impeller system} \quad (6.2\text{-}13)$$

$$Q_{Sn}/Q_{S1}=25.1N^{-0.35}Q_{S1}^{0.17}n_s^{-1.32}(D/T)^{1.54} \quad \text{for PPP impeller system} \quad (6.2\text{-}14)$$

The deviations of all data points are less than 8%.

To examine how the gas recirculation will differ among various impeller combinations in multiple impeller systems, the values of Q_R are calculated for the RRR, PRR, PPR and PPP impeller systems with the same energy dissipation density (P_g/V=1004 W/m^3) and the results are shown in Fig.6.2-8. From the plots shown in these figures, it is found that regardless of the impeller combination, the gas recirculation rate around each impeller always increases with the sparged gas rate initially, and passes through a peak value at a certain sparged gas rate, and approaches zero when the impeller becomes flooded. In the RRR system, since the upper impellers have less sparged gas rate, the top Rushton turbine impeller always gives the highest value of Q_R for almost whole range of Q_{S1}. To have the same energy dissipation density, it needs to increase the rotational speeds of the systems having one or more pitched blade impellers. Therefore, these systems naturally have higher values of Q_R than the RRR system. For the PRR and PPR systems, due to the enforced axial flow from the upper pitched blade impeller, the Rushton turbine impeller just beneath the pitched blade impeller always has the highest value of Q_R. It is worthy to note that Q_R for each impeller in the PPP system is always much lower than those in the other systems and becomes almost zero as impeller tends to be flooded. This result can be attributed to two major reasons: (1) The worse gas dispersion capability of the pitched blade impeller, comparing to the Rushton turbine impeller, results in a more inefficient gas dispersion; (2) because of the axial pumping characteristic of the

pitched blade impeller, the liquid circulating loop generated by each impeller in the PPP system will merge into a single large loop and the upward liquid flow close to tank wall always helps dispersed bubbles to flow upward and gives a smaller gas recirculation rate around each pitched blade impeller.

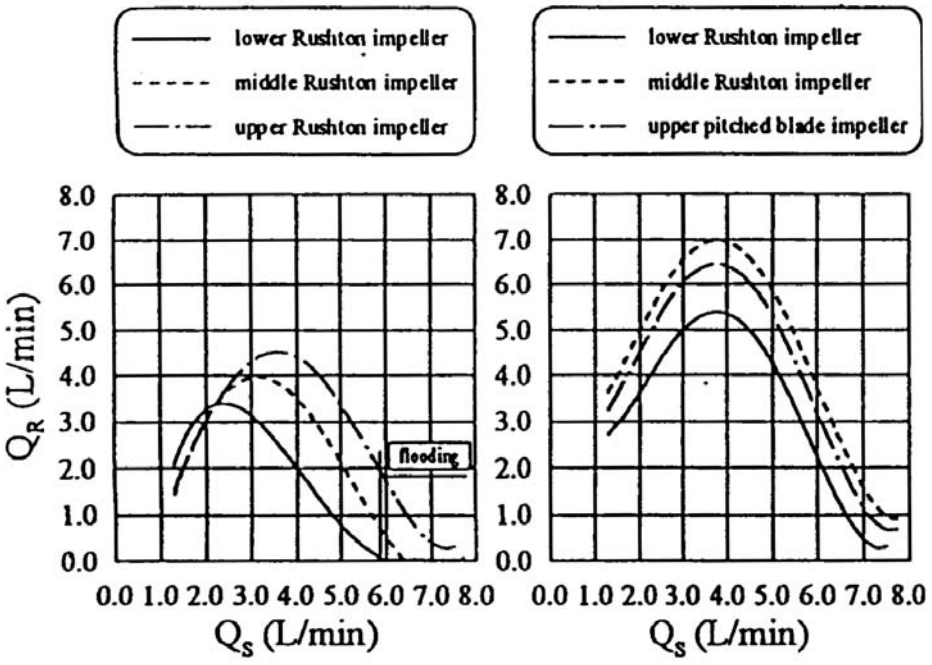

RRR impeller system PRR impeller system

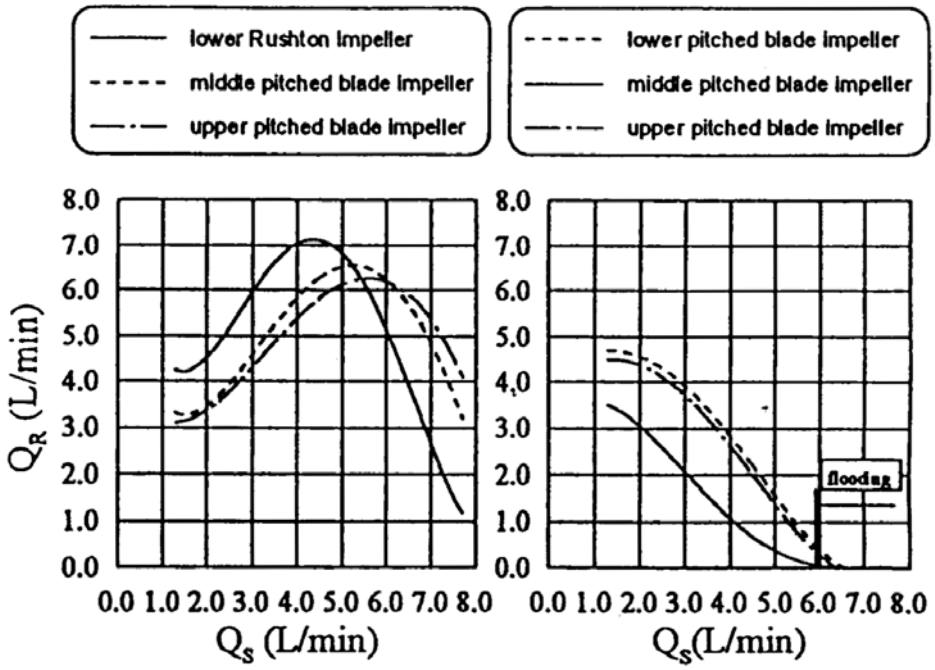

PPR impeller system PPP impeller system

Fig. 6.2-8 The gas recirculation rate around each impeller in multiple impeller system with various impeller combination with P_g/V= 1004.4 W/m^3.

6.3 Estimation of the Power Drawn by Each Impeller in the multiple impeller systems

Evaluating the total gassing rates Q_{tn} around each Rushton turbine impeller in various impeller combination systems by combining Eqs. (6.2-7)-(6.2-8) with Eqs. (6.2-11)-(6.2-13), the value of power drawn by each Rushton turbine impeller $(P_g/P_o)_n$ can be related to the modified aeration number N_A' (=Q_{tn}/ND^3). Two straight lines were obtained for estimating the power drawn data for the Rushton turbine impeller as:

$$(1-P_g/P_o)_n=14.9N_A'=14.9(Q_{tn}/ND^3) \qquad Q_{Sn}/ND^3<0.03 \qquad (6.3\text{-}1)$$

$$(1-P_g/P_o)_n=4.69N_A'+0.432=4.69(Q_{tn}/ND^3)+0.432 \qquad Q_{Sn}/ND^3>0.03 \qquad (6.3\text{-}2)$$

with the flooding condition exclusion. These two correlation equations are discriminated by the value of aeration number Q_S/ND^3. The values of $(1-P_g/P_o)_n$ always increase with the increase in N_A' when the dispersed gas bubbles are circulated well around the whole vessel (i.e. $Q_S/ND^3<0.03$); while as the large cavity embraces the impeller (i.e. $Q_S/ND^3>0.03$), the trend of increasing in $(1-P_g/P_o)_n$ with the increase in N_A' will become more smoothly.

Similar procedure is applied to the pitched blade impeller by using Eqs.(6.2-9)-(6.2-10) and Eqs.(6.2-12)-(6.2-14), and two formulas are proposed to predict the power drawn by each pitched blade impeller in various impeller combination systems under two different gas loading regimes:

$$(1-P_g/P_o)_n=17.91N_A'=17.91(Q_{tn}/ND^3) \qquad Q_{Sn}/ND^3<0.03 \qquad (6.3\text{-}3)$$

and

$$(1-P_g/P_o)_n=3.13N_A'+0.605=3.13(Q_{tn}/ND^3)+0.605 \qquad Q_{Sn}/ND^3>0.03 \qquad (6.3\text{-}4)$$

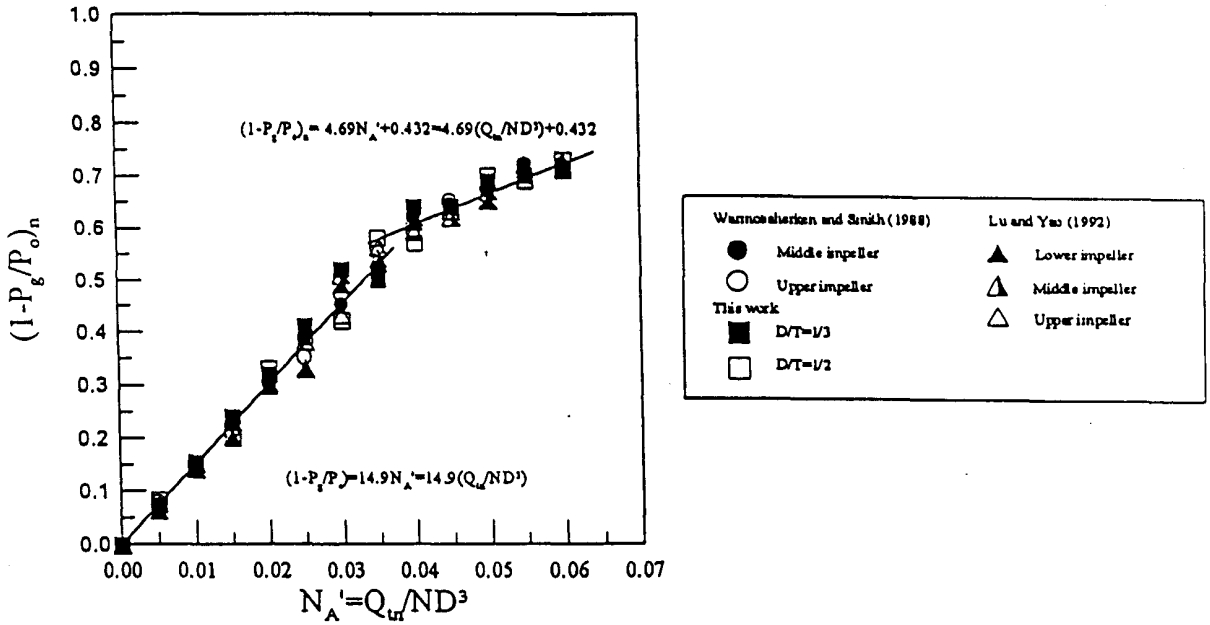

Fig. 6.3-1 Comparison of power drawn data obtained from the literature and the power prediction formula for the Rushton turbine impeller obtained in this study.

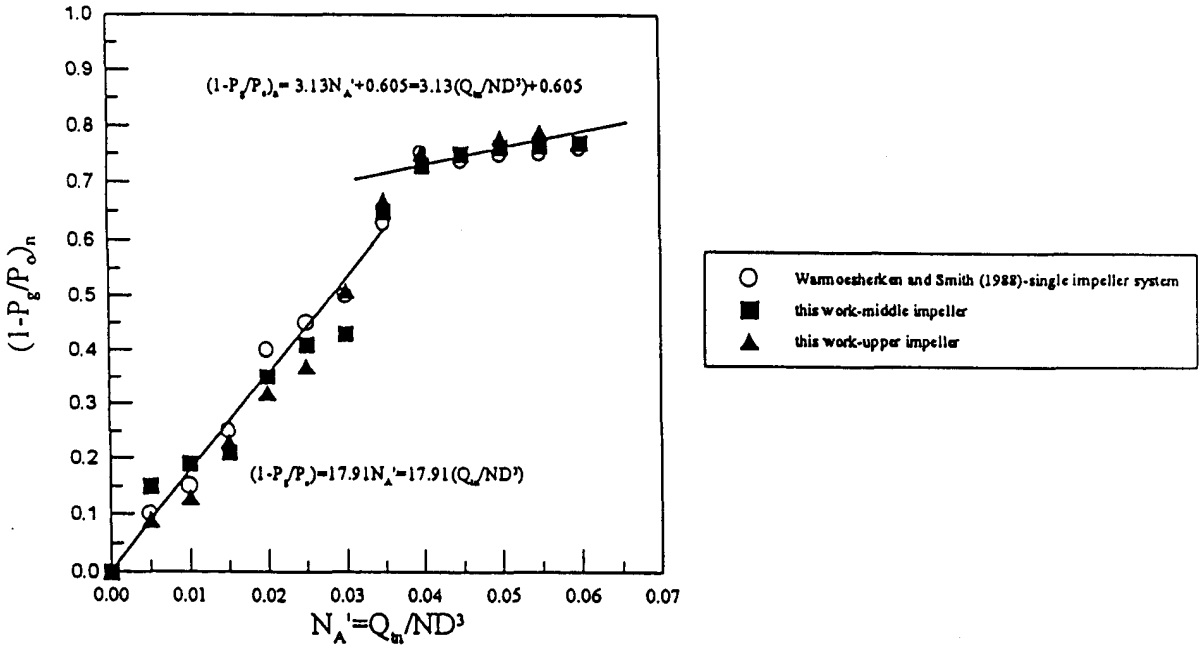

Fig. 6.3-2 Comparison of power drawn data obtained from the literature and the power prediction formula for the pitched blade impeller obtained in this study.

Figures 6.3-1 and 6.3-2 show the regressive results of the correlation equations for estimating the power drawn by the Rushton turbine impeller and the pitched blade impeller, respectively. From the plots depicted in these two figures, it can be found that no matter for the Rushton turbine impeller or the pitched blade impeller, the deviation between the calculated $(1-P_g/P_o)_n$ and these correlations are always less than 15% and all the power drawn data fall into two straight lines according to the value of Q_S/ND^3.

To check the accuracy of the correlation equations for predicting the power drawn by the Rushton turbine impeller and the pitched blade impeller obtained here, the power drawn data obtained from Warmoeskerken & Smith(1988) and Lu & Yao (1992) along with our own experimental data are also plotted in Figs. 6.3-1 and 6.3-2. Where the values of N_A' were evaluated through the correlations in this study based on the N_A values provided by these two previous works. From the data points shown these two figures, it can be seen that although a little larger scatter exists between these correlation equations and data points for some operating conditions, it can be said that these correlation equations can be applied to predict the power drawn by each impeller in multiple impeller systems as a whole. Figure 6.3-3 shows the comparison of the calculated power drawn by the Rushton turbine impeller through Eqs. (6.3-1) and (6.3-2) with the correlation proposed by Michel and Miller (1962). From this figure, it is found that the correlation equations for estimating the power drawn by the Rushton turbine impeller obtained this study were compatible with that proposed by Michel and Miller[2] for all operating conditions, except for the conditions exceed the flooding point.

With the power drawn by each impeller in multiple impeller systems, the total power consumption of each system can be obtained by summing up the power drawn by each individual impeller.

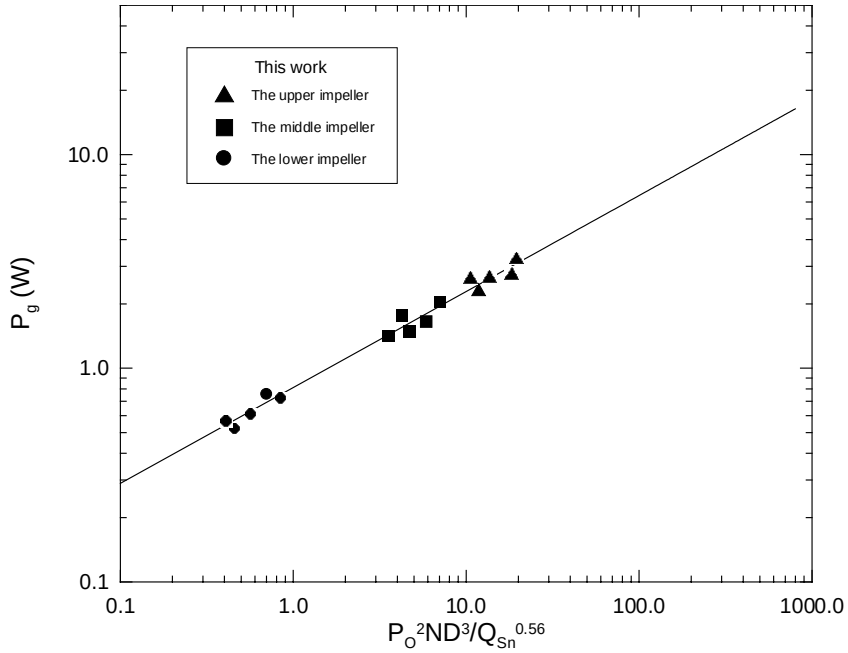

Fig. 6.3-3 Comparison of the calculated power drawn by the Rushton turbine impeller through Eqs. (6.3-1) and (6.3-2) with that proposed by Michel and Miller (1962).

NOTATION

C	Clearance between the impellers	[m]
C_1	Distance between the lowest impeller and tank bottom	[m]
D	Impeller diameter	[m]
Fr	Froud number	[-]
g	Gravitation factor	[m/s^2]
H	Height of liquid free surface	[m]
L	Impeller blade length	[m]
N	Impeller rotational speed	[rps]
N_A	Aeration number(=Q/ND^3)	[-]
N_A'	Modified aeration number(=Q_t/ND^3)	[-]
N_p	Power number(=P/ ρ N^{3}D^5)	[-]
n	Number of blade	[-]
P_g	Power consumption with aeration	[HP]

P_o	Power consumption without aeration	[HP]
Q_R	Gas recirculation rate	[m^3/s]
Q_S	Sparging gas rate	[m^3/s]
Q_t	Total gassing rate(=Q_S+Q_R)	[m^3/s]
Q_{UP}	Uprising gas rate along the take wall	[m^3/s]
R_e	Reynolds number	[-]
T	Tank diameter	[m]
W	Impeller blade width	[m]

<*Greeks Letters*>

α_i	Local gas hold-up	[-]
ε_g	Local gas hold-up	[-]

<*Subscripts*>

n	The n^{th} stage of the impeller	[-]

<*Abbreviation*>

PPP	The system equipped with three pitched blade impellers
PPR	The system equipped with a lower Rushton turbine impeller and two upper pitched blade impellers
PRR	The system equipped with two lower Rushton turbine impeller and a upper Pitched blade impellers
RRR	The system equipped with three Rushton turbine impellers